

3D Lidar Mapping Relative Accuracy Automatic Evaluation Algorithm

Guibin Chen, Jiong Deng, Dongze Huang, Shuo Zhang

Abstract—HD (High Definition) map based on 3D lidar plays a vital role in autonomous vehicle localization, planning, decision-making, perception, etc. Many 3D lidar mapping technologies related to SLAM (Simultaneous Localization and Mapping) are used in HD map construction to ensure its high accuracy. To evaluate the accuracy of 3D lidar mapping, the most common methods use ground truth of poses to calculate the error between estimated poses and ground truth, however it's usually so difficult to get the ground truth of poses in the actual lidar mapping for autonomous vehicle. In this paper, we proposed a relative accuracy evaluation algorithm that can automatically evaluate the accuracy of HD map built by 3D lidar mapping without ground truth. A method for detecting the degree of ghosting in point cloud map quantitatively is designed to reflect the accuracy indirectly, which takes advantage of the principle of light traveling in a straight line and the fact that light can not penetrate opaque objects. Our experimental results confirm that the proposed evaluation algorithm can automatically and efficiently detect the bad poses whose accuracy are less than the set threshold such as 0.1m, then calculate the bad poses percentage \mathcal{P}_{bad} in all estimated poses to obtain the final accuracy metric $\mathcal{P}_{acc} = 1 - \mathcal{P}_{bad}$.

I. INTRODUCTION

In recent years, with the rise of AI (Artificial Intelligent), autonomous driving technology has been greatly developed. The HD map with centimeter level accuracy plays an important role in the localization, planning, decision-making and perception of autonomous vehicles, which is usually built by 3D lidar mapping algorithm. After the HD map has been constructed, we need to evaluate its accuracy to improve the related mapping algorithm or check whether the HD map meets the accuracy requirement of actual use.

A. Problem Description

As everyone knows, the process of mapping is that sequences of 3D point clouds are transformed from body coordinate system to world coordinate system according to their corresponding estimated poses, so evaluating the map accuracy is actually evaluating the estimated poses accuracy, which is based on the premise that all 3D point clouds have been removed the distortion caused by vehicle movement and lidar rotation through the motion compensation algorithm. The accuracy of pose is usually divided into absolute accuracy and relative accuracy, the former is usually not ambiguous, but the latter has different meanings in different papers. In this paper, the relative accuracy refers to the relative position accuracy between different poses, which is usually presented by the degree of ghosting in the point

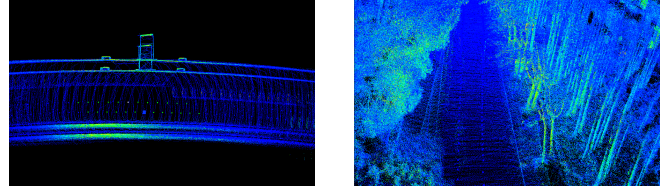


Fig. 1: Serious ghosting phenomenon of point cloud map in tunnel and campus scenes. This problem is mainly caused by a large error in relative position between the different poses, and those poses are called bad poses with low relative accuracy in this paper.

cloud map: the lower the relative accuracy of poses, the more serious the ghosting problem of the point cloud map, and the more unfavorable it is for online localization algorithm based on point cloud matching.

In the field of autonomous driving, the accuracy evaluation metric of the HD map is usually expressed by the percentage \mathcal{P}_{acc} : percentage of poses with relative accuracy greater than 0.1m in all estimated poses. The bad poses with relative accuracy less than 0.1m will cause serious ghosting in the corresponding areas of point cloud map as shown in Fig. 1, which will gravely affect many functions based on HD map for autonomous vehicles, such as online localization. In this paper we also use the percentage \mathcal{P}_{acc} as one of the output of our algorithm to describe the relative accuracy of 3D lidar mapping quantitatively.

The most common algorithms of map accuracy evaluation generally use ground truth of poses to calculate the error between estimated poses and ground truth, which belong to the field of absolute accuracy evaluation. But when the 3D lidar mapping algorithm is applied to the daily production of HD map, the ground truth of poses are usually not available, and to the best of authors knowledge, the 3D lidar mapping accuracy evaluation algorithm without ground truth is rarely studied in the academic and industry field which belongs to relative accuracy evaluation. The algorithm proposed in our paper is to solve this problem.

B. Challenges

Although we realize that when there is no ground truth of poses, we can only reflect the relative accuracy of the 3D point cloud map through the degree of possible ghosting in map, it's still not easy to automatically and efficiently detect and measure the ghosting. One of the challenges is the efficiency of the ghosting detection, nowadays, many HD map manufacturers check the accuracy of map by manual sampling inspection, but too few samples can not reflect the real situation of the map accuracy; too many samples will cost a lot of manpower or lead to low efficiency of map

quality assessing. Another challenge is to detect the map ghosting along the three directions of XYZ axis. There is a method in the industry to evaluate the map relative accuracy by calculating the ground thickness in the point cloud map, but this method can only detect the ghosting along the Z axis (assuming that the Z axis is perpendicular to the ground). Similarly, the method of detecting the map ghosting along the XY axis through the thickness of traffic sign or lamp-post has theoretical defect: the thickness of traffic sign or lamp-post has no definite value which is different from the thickness of the ground.

C. Related Works

In order to assess the quality of mapping algorithms, the most common methods are to obtain the ground truth of poses, then calculate the APE (Absolute Pose Error) between estimate and reference [1] [2], so, lots of related research works are focused on how to obtain the ground truth of poses. In [3] and [4], the authors used the output of the GPS-IMU localization unit or the GNSS-RTK measurement as the ground truth for visual or lidar odometry/SLAM. However, these kinds of integrated navigation algorithms can't provide reliable ground truth poses in the area with poor satellite signal, which is caused by the shelter of tall buildings or trees. Based on the fact that lidar SLAM are usually 10 times more accurate than visual SLAM, [5] obtained the ground truth camera trajectory composed by poses through a lidar-based SLAM system since the relative transformation between lidar and camera is known by calibration.

In addition to obtain the ground truth of poses, some works are dedicated to building the ground truth map by employing professional surveying and mapping device equipped with redundant sensors [6] [7]. Some accuracy evaluation algorithms need manual operation, for example, [8] required manually matching point cloud observed by lidar to avoid point cloud registration failure.

However, all the above methods are aimed at establishing benchmarks, which are usually used to compare the results of different mapping algorithms or improve the researchers' mapping algorithms. As far as the authors know, few work studies accuracy evaluation without ground truth when mapping (especially for 3D lidar mapping) algorithms are applied to the actual production of HD map. In this case, we can only indirectly calculate the relative accuracy of the map by detecting the map's overlap or ghosting. [9] mainly selected three kinds of geometric feature metrics to determine the 2D map's quality without the ground truth of poses or map: the proportion of free and occupied cells, the number of the corners and the enclosed areas, but those metrics are not suitable for 3D lidar mapping in outdoor scenes because the 3D point clouds in these scenes are usually unevenly distributed and their geometry is often irregular. In [10], the authors suppose that there are many planar structures in the environment and segment the 3D point cloud map into plane patches, then check whether the following two types of suspicious plane appear: the intersecting plane patches that don't represent corners and the parallel plane patches

very close to each other, which indicates that the map at the suspicious plane appears ghosting, and its relative accuracy there is relatively low. However, [10] mainly measures the quality of 3D laser map in urban environment where many artificial planar structures such as buildings exist. Once there are only some pole-like objects in some scenes, this algorithm would not work.

In contrast to all the above accuracy evaluation approaches, we focus on designing a more general 3D lidar mapping relative accuracy automatic evaluation algorithm without the ground truth of poses or map by assessing the degree of ghosting in 3D point cloud map, where the map's ghosting is actually caused by the translation or rotation relative error of the related estimated poses.

II. PROBLEM STATEMENT

The input of our designed accuracy evaluation method is a sequence of estimated poses set $\mathcal{T} = \{\mathbf{T}_i \mid i = 1, \dots, n\}$ and 3D point clouds set $\mathcal{C} = \{\mathcal{C}_i \mid i = 1, \dots, n\}$, where each pose $\mathbf{T}_i \in SE(3)$ is a transformation matrix estimated by 3D lidar mapping algorithm and each point cloud \mathcal{C}_i is a set of 3D points $\{\mathbf{P}_j \mid j = 1, \dots, m\}$ observed by multi-line 3D lidar such as Velodyne's HDL-32E and has been motion compensated to correct distortion. Each point $\mathbf{P}_j \in \mathbb{R}^5$ is a vector of its coordinate under body coordinate system (e.g. vehicle coordinate system) $P_j(x, y, z)$ plus its scanID and fireID (s, f) which represents the vertical and horizontal firing order of 3D lidar's lasers respectively. Pose \mathbf{T}_i and point cloud \mathcal{C}_i have been synchronized in time, so they have a one-to-one correspondence.

Our proposed method outputs the indices set \mathcal{S}_b of bad poses whose relative accuracy are less than the set threshold 0.1m, $\mathcal{S}_b \subseteq \{i \mid i = 0, \dots, n - 1\}$. Our method also outputs the relative accuracy evaluation metric: percentage $\mathcal{P}_{acc} = 1 - \mathcal{P}_{bad}$, where \mathcal{P}_{bad} is the percentage of bad poses in all input estimated poses. With an easy visualization tool based on PCL viewer, we can utilize the input and output data to view the ghosting situation of the point cloud submap around the bad poses, like the video we provided.

III. PROPOSED METHOD

A. Map Ghosting Detection Principle

Without the ground truth of poses or map, the intuitive way to judge the accuracy of a point cloud map constructed by 3D lidar mapping algorithm is to detect whether the ghosting appears in the map as in Fig. 1. Our basic principle of detecting map ghosting is based on the fact that laser of 3D lidar travels in a straight line and can not penetrate opaque objects, which is often used for ray tracing, dynamic elements identification or estimating the quality of point cloud alignment by some researchers [11] [12] [13].

Fig. 2 shows an example of our method to detect ghosting: For pose \mathbf{T}_i , we first transform its corresponding point cloud \mathcal{C}_i from body coordinate system to world coordinate system to get point cloud \mathcal{C}_i^W , then search for poses near the pose \mathbf{T}_i with a certain radius r_s , also transform their corresponding point clouds into world coordinate system to make up the

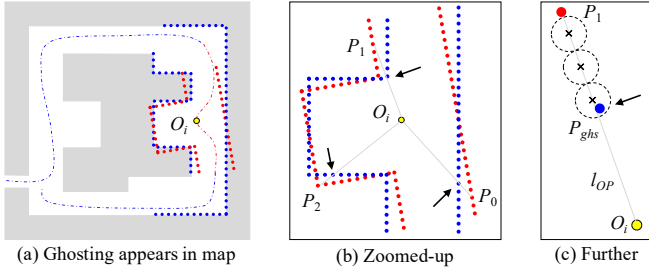


Fig. 2: An example of detecting ghosting in plan view. Red and blue points represent point cloud C_i^W and submap C_s^W respectively and we have not shown the ground points for display convenience. Dash-dotted line is trajectory composed by poses, where the red part represents the poses near the pose T_i . In (b) (c), the gray solid line denote the line l_{OP} , and the black arrows emphasize the ghosting points. The black cross marks in (c) indicate the selected sampling positions and the black dashed circles around them represent the detection range r_{ghs} .

submap C_s^W . If submap C_s^W don't contain ghosting, then there should be no points of C_s^W on line l_{OP} from the lidar observation center O_i to every point P_j of C_i^W . If not, ghosting point P_{ghs} is detected and we call that the ghosting point P_{ghs} is captured by the point P_j .

In order to discretize the above-mentioned ghosting detection process to facilitate programming, we select some sampling positions on line l_{OP} starting from the end of point P_j , and only detect ghosting points at these positions, as shown in Fig. 2(c).

Obviously, the proposed principle of ghosting detection will be broken by dynamic obstacles, so we will use some 3D obstacle perception algorithms [14] [15] to remove them.

B. Metric of Ghosting in Point Cloud Map

In order to calculate the relative accuracy of pose T_i , we first need to quantitatively describe the blur degree of ghosting detected in 3D point cloud map, where the required lidar observation center O_i can be obtained by pose T_i and the calibration parameters from body coordinate system to lidar coordinate system.

Considering the measurement error ($1 \sim 2cm$, usually) of the 3D lidar sensor, we set a threshold d_{thre} to determine whether the ghosting point P_{ghs} is located on line l_{OP} , and the ghosting detection range r_{ghs} should be slightly larger than the threshold d_{thre} . The basic quantized metric d_{ghs} of ghosting is shown in Fig. 3.

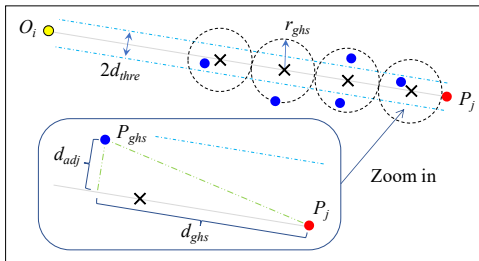


Fig. 3: Illustration of the basic quantized metric d_{ghs} of ghosting. The two cyan dash-dotted lines show the tolerance of judging whether the ghosting point P_{ghs} is located on line l_{OP} , and the other marks are same to Fig. 2.

To improve the search efficiency, we build the submap C_s^W into a kd-tree, and use its radius search function to search for ghosting points within radius r_{ghs} at each sampling location. Once searched, the euclidean distance d_{adj} is calculated by

$$d_{adj} = \frac{|\overrightarrow{O_i P_j} \times \overrightarrow{P_{ghs} P_j}|}{|\overrightarrow{O_i P_j}|} \quad (1)$$

If $d_{adj} < d_{thre}$, we determine that the searched ghosting point is located on line l_{OP} , so the basic quantized metric d_{ghs} of ghosting given by

$$d_{ghs} = \frac{\overrightarrow{O_i P_j} \cdot \overrightarrow{P_{ghs} P_j}}{|\overrightarrow{O_i P_j}|} \quad (2)$$

is valid, and vice versa.

However, the above basic metric d_{ghs} can not exactly measure the ghosting appeared in point cloud map when line l_{OP} is nearly parallel to the surface S_j where the point P_j is located, as shown in Fig. 4. Thus, we must estimate the normal vector n_j of surface S_j to get the more precise metric d_{prj} of ghosting to solve this problem.

Using the established kd-tree of submap C_s^W , we can easily obtain the point cloud C_j^s in the vicinity of surface S_j and then calculate the normal vector n_j by PCA (Principal Component Analysis), mainly as follows:

$$\begin{aligned} \bar{P} &= \frac{1}{k} \sum_{i=1}^k P_i, \forall P_i(x, y, z) \in C_j^s \\ \mathbf{A}_{cor} &= \frac{1}{k} \sum_{i=1}^k (P_i - \bar{P})(P_i - \bar{P})^T, \mathbf{A}_{cor} \in \mathbb{R}^{3 \times 3} \\ \mathbf{A}_{cor} \mathbf{V} &= \lambda \mathbf{V}, \text{ solved by SVD, } \lambda(\lambda_0 < \lambda_1 < \lambda_2) \end{aligned} \quad (3)$$

where the eigenvalue λ_0 of the covariance matrix \mathbf{A}_{cor} is significantly smaller than the other two eigenvalues λ_1, λ_2 , since the point cloud C_j^s is approximately distributed on a planar patch. The eigenvector v_0 in $\mathbf{V}(v_0, v_1, v_2)$ corresponding to the minimum eigenvalue λ_0 denotes the normal vector of the planar patch: $n_j = v_0$.

Because the above problem only occurs when line l_{OP} is approximately perpendicular to normal vector n_j of surface

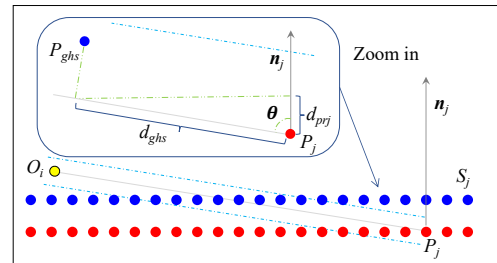


Fig. 4: Front view of the ground point cloud used to illustrate the more precise metric d_{prj} of ghosting. The Blue and red points represent the ground in submap C_s^W and point cloud C_i^W respectively, and the brown up arrow above point P_j indicates the normal vector of the ground surface.

S_j , so we calculate the angle θ between l_{OP} and \mathbf{n}_j by

$$\theta = \arccos \frac{\overrightarrow{O_i P_j} \cdot \mathbf{n}_j}{|\overrightarrow{O_i P_j}| |\mathbf{n}_j|} \quad (4)$$

and combine d_{adj} to switch the final metric d_{prj} of ghosting

$$d_{prj} = \begin{cases} d_{ghs} * \cos \theta, & \text{if, } d_{adj} < d_{thre} \\ & \text{and, } \theta > \theta_{thre} \\ d_{ghs}, & \text{elseif, } d_{adj} < d_{thre} \\ 0, & \text{otherwise} \end{cases} \quad (5)$$

If we perform the above-mentioned ghosting detection on each point of the point cloud C_i^W and measure the detected ghosting points by the metric d_{prj} , the time-consuming of our entire 3D lidar mapping relative accuracy automatic evaluation algorithm will be terrible, because the original point cloud C_i of point cloud C_i^W usually contains tens of thousands of points, so we need to downsample the point cloud C_i and submap C_s^W through some certain strategies.

C. Point Cloud Downsampling Method

The main problem with submap C_s^W is that the point cloud is generally very dense due to the superposition of multiple point clouds, so we downsample it directly by the voxel grid filter with leaf size 0.02m.

However, the downsampling process of point cloud C_i is relatively complicated. On the one hand, the spatial position of the points in C_i can not be changed during the downsampling, otherwise the basic principle of ghosting detection will be broken; On the other hand, the spatial distribution of a single-frame laser point cloud like C_i is very uneven, and the ground points occupy most of the points near the lidar observation center O_i , but we do not want too many ground points to participate in ghosting detection; In addition, we hope to keep all the pole-like points during the downsampling, which will facilitate ghosting detection in the scene where buildings are missing and only some trees.

So first, we extract the ground and pole-like points from the point cloud C_i in body coordinate system through semantic segmentation of point cloud based on deep learning [16], and set the corresponding points label to “ground” and “pole”, and the other points label to “default”.

After obtaining the simple semantic information, we use the scanID and fireID of points in C_i to solve the problem that point cloud is dense in the middle and sparse in the outer, and finally realize the relatively uniform downsampling in space for point cloud C_i through the method summarized in Alg. 1. The effect is shown in Fig. 5.

D. Calculate the Relative Accuracy of Pose

Using the downsampled submap C_s^W and point cloud $C_i^W = T_i C_i^d$, we run the ghosting detection method and will get a series of ghosting points with metric d_{prj} . In order to determine whether the relative accuracy of pose T_i reaches 0.1m, we first need to record some statistics:

- the labeled “pole” points number n_{pole} in the downsampled point cloud C_i^W ;

Algorithm 1: downsampling for point cloud C_i

```

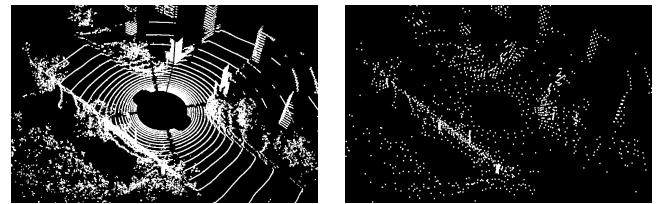
Input: original point cloud  $C_i$ 
Output: downsampled point cloud  $C_i^d$ 
Every Point  $P \in C_i$  has members  $(x, y, z, s, f, l)$ , which represent
its coordinate, scanID, fireID, label, respectively.
 $n_l$  is the lasers number of the 3D lidar sensor.
 $\theta_r$  is the horizontal angular resolution( $^\circ$ ) of lidar.
Let  $f_m = 360/\theta_r$ , and  $\xi = f_m/n_l$ .
So  $P(s)$  range  $0, 1, \dots, n_l - 1$ ;  $P(f)$  range  $0, 1, \dots, f_m - 1$ .
Set  $\eta_{ground} = 30/\theta_r$ .
Set  $\eta_{vec} = \{ \{5, 6/\theta_r\}, \{10, 4/\theta_r\}, \{20, 2/\theta_r\}, \{900, 1/\theta_r\} \}$ .
Init  $C_i^d$  empty.
foreach  $P \in C_i$  do
  if  $P(l) = \text{“pole”}$  then
    | push  $P$  to  $C_i^d$ 
  else
    |  $f_{scat} = P(f) + P(s) * \xi$ 
    | if  $f_{scat} \geq f_m$  then
    | |  $f_{scat} = f_{scat} - f_m$ 
    | end
    | if  $P(l) = \text{“ground”}$  and  $f_{scat} \% \eta_{ground} = 0$  then
    | | push  $P$  to  $C_i^d$ 
    | else
    | | foreach  $\eta \in \eta_{vec}$  do
    | | | if  $\|P(x, y, z)\| < \eta.first$  and
    | | | |  $f_{scat} \% \eta.second = 0$  then
    | | | | | push  $P$  to  $C_i^d$ 
    | | | | | break
    | | | end
    | | end
    | end
  end
end
return  $C_i^d$ 

```

- the total number n_{ordi} of the labeled “ground” or “default” points in C_i^W ;
- the number m_{pole} of the ghosting points with metric $d_{prj} > 0.1m$ which are captured by the labeled “pole” points in C_i^W ;
- the number m_{ordi} of the ghosting points with metric $d_{prj} > 0.1m$ which are captured by the labeled “ground” or “default” points in C_i^W .

Then, if $m_{pole}/n_{pole} > t_{pole}$ or $m_{ordi}/n_{ordi} > t_{ordi}$ where t_{pole} and t_{ordi} is the set threshold, we can determine that the pose T_i is a bad pose and insert the pose index i to the bad poses indices set S_b .

After completing the relative accuracy evaluation to all the estimated poses in \mathcal{T} , our method outputs the indices set S_b and calculates the percentage \mathcal{P}_{bad} of the detected bad poses in \mathcal{T} to present the relative accuracy evaluation metric: $\mathcal{P}_{acc} = 1 - \mathcal{P}_{bad}$.



(a) before downsampling

(b) after downsampling

Fig. 5: The effect of downsampling for single-frame point cloud C_i .

IV. EXPERIMENTS

Our method evaluates the 3D lidar mapping relative accuracy through detecting the bad poses whose relative accuracy are less than 0.1m in the trajectory produced by the mapping algorithm and calculating their percentage in all estimated poses. However, all detection algorithms have a trade-off between the precision and recall rate. For the map accuracy evaluation problem in this paper, we are more inclined to have a higher recall rate of bad poses detection, and we achieved this by tuning some threshold parameters in the proposed accuracy evaluation algorithm.

In order to test the practical application effect of our algorithm, we need to experimentally verify the precision and recall rate of the bad poses detection. To this end, we first obtain ground truth poses in four different real-world scenes by running a 3D lidar mapping algorithm, which is based on LOAM [17] and uses the output of integrated navigation device to perform a loop detection in the back end. After offline pose graph optimization and some necessary manual correction, the relative accuracy of ground truth poses can reach more than 0.03m.

A. Precision Rate Verification

The precision verification experiment is relatively simple: we directly apply our method to evaluate the relative accuracy of the ground truth poses in the four benchmark scenes. Because the ground truth poses have extremely high relative accuracy, once our method detects bad pose, it is a false detection, therefore, the metric \mathcal{P}_{acc} output by our method is exactly the precision rate that needs to be verified in this experiment. The result is shown in Tab. I which indicates that the precision rate of our designed relative accuracy evaluation algorithm is greater than 98%.

B. Recall Rate Verification

In order to verify the recall rate of our method to detect bad poses, we need to artificially add some disturbances to the ground truth poses to intentionally generate ghosting in specified areas on the point cloud map. Meanwhile, we add disturbances to the xy or z value of ground truth poses separately to prove that our method can detect both the horizontal and vertical ghosting distributed along the XY and Z axis.

Fig. 6 shows the specific way to add the disturbances: artificially add 0.1, 0.15, 0.2m disturbances to the xy value

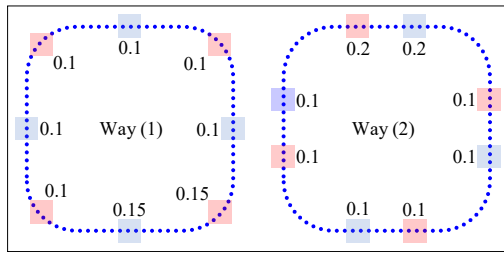


Fig. 6: The specific way of adding disturbances to the ground truth poses. Blue dotted line is the trajectory, and the upper red or blue rectangles indicate the areas where disturbances are added in the XY or Z direction. Numbers near the rectangles represent the magnitude of the disturbances.

or z value of ground truth poses in specified areas of the trajectory according to the proportion of 6 : 1 : 1, and the length of each disturbance is 50m.

We perform our accuracy evaluation method in the four different benchmark scenes where the artificially set disturbances are added through the way (1) and way (2) as illustrated in Fig. 6, and considering that one disturbed pose will cause ghosting in its surrounding point cloud submap, we use the area with disturbance as the statistical unit to calculate the recall rate.

The experimental result is shown in Tab. II, and we can see that the recall rate for detecting the areas with disturbance of our proposed method is 100%. This is mainly due to that we specially adjust some threshold parameters to improve the recall rate, which is actually at the expense of the precision rate. And Fig. 7 shows the visualization results of the experiments executed in benchmark scene 0 which is an office park in the real world. More visualization information can be seen in the provided video.

C. Discussion

During evaluating the relative accurate for 3D lidar mapping, we just rely on detecting and measuring the possible ghosting in the point cloud map. However, in the actual application, we found that low bushes and some lush leaves would cause our algorithm to falsely detect ghosting points. Of course, this is taken for granted in the view of our basic principle of detecting ghosting as shown in Fig. 2, because the same leaf or the same willow branch is really hard to remain stationary during multiple map collections and it can easily be blown by the wind to change its position in space. But this phenomenon will affect the precision rate of our algorithm in detecting bad poses.

Therefore, in addition to the simple semantic information of the ground and pole-like points, more point cloud semantic information would be used to reduce the adverse impact of bushes or lush leaves on our proposed method.

V. CONCLUSIONS

In this paper, we proposed a novel method to automatically evaluate the relative accuracy for 3D lidar mapping without the ground truth of poses or map. By detecting and measuring the ghosting in the submap around the pose to be evaluated, we can indirectly judge whether it is a bad

TABLE I: Result of precision rate verification

Scene sequence	Distance (km)	Number of poses	Time cost (min)	Precision (%)
0	5.24	4580	24	99.13
1	13.7	16818	45	99.48
2	22.8	11466	63	98.12
3	7.2	6325	29	98.03

The used hardware condition: an Intel(R) Core(TM) i7-8700 CPU with 6 cores @ 3.20GHz with 32 GB RAM, and a Nvidia GeForce GTX 1080 with 8 GB RAM. And the time cost were tested on 10 threads.

TABLE II: Result of recall rate verification

Direction of disturbance		XY	Z	XY	Z	XY	Z	XY	Z	XYZ
Scene sequence	Distance (km)	Number of areas with 0.1m disturbance		Number of areas with 0.15m disturbance		Number of areas with 0.2m disturbance		Total number of all the areas		Recall (%)
0	5.24	6	6	1	1	1	1			
1	13.7	6	6	1	1	1	1	32	32	100
2	22.8	6	6	1	1	1	1			
3	7.2	6	6	1	1	1	1			

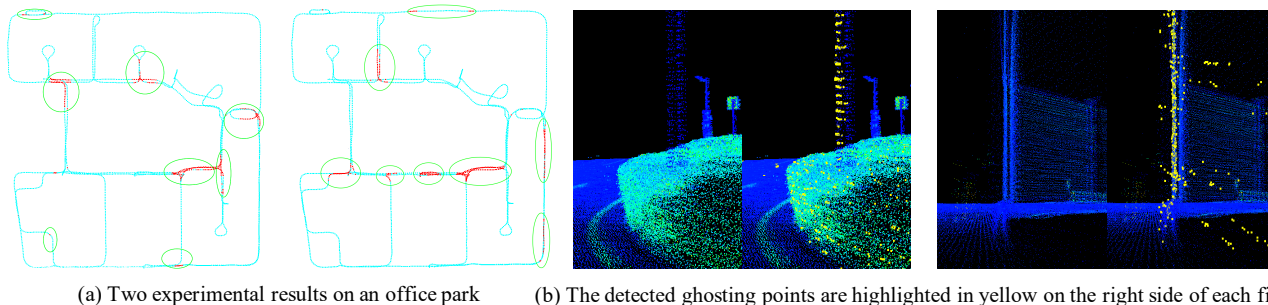


Fig. 7: Visualization results of partial recall rate experiments. (a) shows the trajectories of the accuracy evaluation results after adding disturbances according to the way (1) and way (2) illustrated in Fig. 6, where the red and cyan points represent the detected bad poses and the normal poses respectively, the green oval circles represent the ground truth of the perturbed areas. (b) shows the detected ghosting points which are colored yellow and located in the submap around some bad poses shown in (a).

pose whose relative accuracy is less than 0.1m. Thus our method finally calculates the percentage \mathcal{P}_{bad} of bad poses in all estimated poses and then outputs the common evaluation metric $\mathcal{P}_{acc} = 1 - \mathcal{P}_{bad}$ of the HD map for autonomous vehicles. We built four real-world benchmark map data to verify the precision and recall rate of detecting bad poses by our method, the experimental results demonstrate that the precision rate is greater than 98% and the recall rate is 100%. Moreover, our method can realize the 3D accuracy evaluation of poses by detecting the ghosting distributed along the three axes of XYZ, and the whole evaluation process is fully automated which greatly reduces the labor cost of quality inspection for HD map. The efficiency of our method in the hardware condition mentioned in this paper is up to $3.3min/km$, which can be further improved once the method is parallelized on a larger scale. In the future, we will use more point cloud semantic information to improve the precision rate and robustness of our method.

REFERENCES

- [1] M. Grupp, “evo: Python package for the evaluation of odometry and slam.” <https://github.com/MichaelGrupp/evo>, 2017.
- [2] Z. Zhang and D. Scaramuzza, “A tutorial on quantitative trajectory evaluation for visual (-inertial) odometry,” in *2018 IEEE/RSJ International Conference on Intelligent Robots and Systems (IROS)*, pp. 7244–7251, IEEE, 2018.
- [3] A. Geiger, P. Lenz, and R. Urtasun, “Are we ready for autonomous driving? the kitti vision benchmark suite,” in *2012 IEEE Conference on Computer Vision and Pattern Recognition*, pp. 3354–3361, IEEE, 2012.
- [4] A. Salach, K. Bakula, M. Pilarska, W. Ostrowski, K. Górski, and Z. Kurczyński, “Accuracy assessment of point clouds from lidar and dense image matching acquired using the uav platform for dtm creation,” *ISPRS International Journal of Geo-Information*, vol. 7, no. 9, p. 342, 2018.
- [5] T. Caselitz, B. Steder, M. Ruhnke, and W. Burgard, “Monocular camera localization in 3d lidar maps,” in *2016 IEEE/RSJ International Conference on Intelligent Robots and Systems (IROS)*, pp. 1926–1931, IEEE, 2016.
- [6] H. Chen, X. Zhao, J. Luo, Z. Yang, Z. Zhao, H. Wan, X. Ye, G. Weng, Z. He, T. Dong, *et al.*, “Towards generation and evaluation of comprehensive mapping robot datasets,” *arXiv preprint arXiv:1905.09483*, 2019.
- [7] Y. Chen, J. Tang, C. Jiang, L. Zhu, M. Lehtomäki, H. Kaartinen, R. Kaijaluoto, Y. Wang, J. Hyypä, H. Hyypä, *et al.*, “The accuracy comparison of three simultaneous localization and mapping (slam)-based indoor mapping technologies,” *Sensors*, vol. 18, no. 10, p. 3228, 2018.
- [8] R. Kümmerle, B. Steder, C. Dornhege, M. Ruhnke, G. Grisetti, C. Stachniss, and A. Kleiner, “On measuring the accuracy of slam algorithms,” *Autonomous Robots*, vol. 27, no. 4, p. 387, 2009.
- [9] A. Filatov, A. Filatov, K. Krinkin, B. Chen, and D. Molodan, “2d slam quality evaluation methods,” in *2017 21st Conference of Open Innovations Association (FRUCT)*, pp. 120–126, IEEE, 2017.
- [10] M. Chandran-Ramesh and P. Newman, “Assessing map quality using conditional random fields,” in *Field and Service Robotics*, pp. 35–48, Springer, 2008.
- [11] A. S. Glassner, *An introduction to ray tracing*. Elsevier, 1989.
- [12] F. Pomerleau, P. Krüsi, F. Colas, P. Furgale, and R. Siegwart, “Long-term 3d map maintenance in dynamic environments,” in *2014 IEEE International Conference on Robotics and Automation (ICRA)*, pp. 3712–3719, IEEE, 2014.
- [13] L. Ding and C. Feng, “Deepmapping: Unsupervised map estimation from multiple point clouds,” in *Proceedings of the IEEE Conference on Computer Vision and Pattern Recognition*, pp. 8650–8659, 2019.
- [14] B. Li, T. Zhang, and T. Xia, “Vehicle detection from 3d lidar using fully convolutional network,” *arXiv preprint arXiv:1608.07916*, 2016.
- [15] B. Wu, A. Wan, X. Yue, and K. Keutzer, “SqueezeSeg: Convolutional neural nets with recurrent crf for real-time road-object segmentation from 3d lidar point cloud,” in *2018 IEEE International Conference on Robotics and Automation (ICRA)*, pp. 1887–1893, IEEE, 2018.
- [16] C. R. Qi, L. Yi, H. Su, and L. J. Guibas, “Pointnet++: Deep hierarchical feature learning on point sets in a metric space,” in *Advances in neural information processing systems*, pp. 5099–5108, 2017.
- [17] J. Zhang and S. Singh, “Loam: Lidar odometry and mapping in real-time,” in *Robotics: Science and Systems*, vol. 2, 2014.